Supporting Information

for

Impact of the lipid bilayer membrane on energy transfer kinetics in the photosynthetic protein LH2

John Ogren,[‡a] Ashley Tong,[‡a] Samuel Gordon,[a] Aurelia Chenu,[a] Yue Lu,[b] Robert Blankenship,[b] Jianshu Cao, [a] and Gabriela Schlau-Cohen[*a]

[a] Department of Chemistry, Massachusetts Institute of Technology, Cambridge, MA 02139

[b] Department of Biology and Chemistry, Washington University in St. Louis, One Brookings Drive, St. Louis, MO 63130

‡ These authors contributed equally to this work

* Corresponding Author: gssc@mit.edu

Spectroscopy system layout

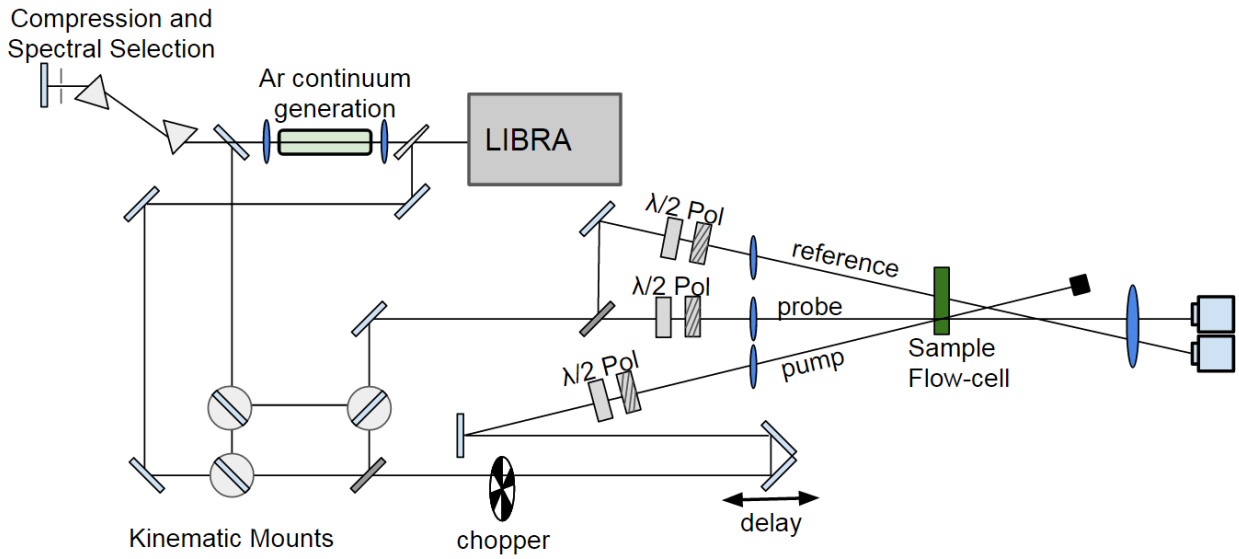

Figure 1 Schematic drawing of the transient absorption spectroscopy system in the Schlau-Cohen lab.

1 Transient absorption apparatus

The output of the regenerative amplifier (Libra, Coherent: 800 nm 40 fs, 5 kHz, 1 mJ per pulse), is split into two pulses. The pulse reflected off of the front face of the wedge (see SI figure S1) is used as the pump and probe for experiments using laser pulses centered at 800 nm while the transmitted pulse is used in 850 nm pulse generation, as discussed below. For one-color experiments, the pulse is steered through a beamsplitter where the pump and probe arms are generated. The pump arm is chopped to 1/2 repetition rate (2.5 kHz) and is delayed relative to the probe pulse by a retroreflector on a translation stage. This translation stage has 1 μm minimum step size, which equates to $\sim$6.7 fs of time delay. The probe beam is split with a second beamsplitter to generate the probe (reflected) and the reference (transmitted) pulses. All three beams have independent waveplate-polarizer pairs to control power and polarization. All three beams go through 400 mm focusing lenses and the pump and probe beams are focused at the sample position with a crossing angle of $<10^{o}$. The reference beam is offset horizontally from the pump-probe overlap position by 3 mm. The spot size at the sample is 100 μm. After the sample, the pump is blocked and the probe and reference beams are recollimated with a 250 mm lens and detected on two photodiodes (Thorlabs).

For transient absorption experiments, the signals from the probe detector and from the

reference detector are sent to the A and B channels of one lock-in amplifier and the lock-in is run in differential mode. The phase independent lock-in intensity is recorded via GPIB communication using a LabView program that also controls the delay stage. For transient anisotropy measurements, the signals from the probe and reference detectors are simultaneously measured via two separate lock-in amplifiers.

2 850 nm pulse generation

The output of the regenerative amplifier is sent through a waveplate-polarizer (Meadowlark Optics) pair that sets the power to 3 W and is focused with a 1 m focal length lens into a tube of Argon to generate a high power supercontinuum. The Argon tube is held at 22 psi and has Brewster plate windows at the entrance and exit to minimize reflections. The tube is $\sim$1 meter long and the focal spot is located 60 cm from the entrance window. The supercontinuum output is collimated with a 750 mm lens and sent into a prism compressor comprised of a double pass through a pair of fused silica prisms (Edmunds Optics). After the first pass the dispersed continuum is spatially filtered with a razor blade to select for 850 $\pm$ 20 nm. The pulse duration is measured to be $<$50 fs via SHG FROG at the sample position.

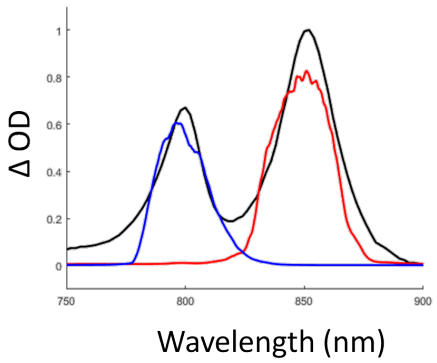

Figure 2 LH2 absorption spectrum of the B800 and B850 bands. The 800 nm regenerative amplifier output is shown in blue and the spectrally filtered supercontinuum pulse centered at 850 nm is shown in red.

3 Power dependence measurements

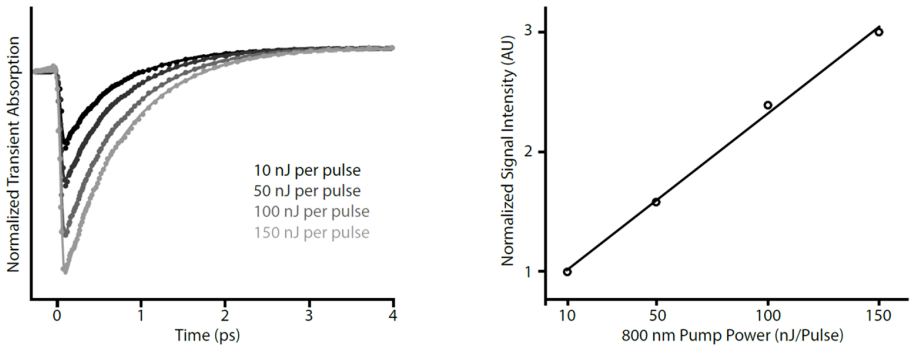

Figure 3 Power dependence data for the 800 pump - 800 probe data. Left: Magic angle data were acquired for LH2 solubilized in LDAO which were in agreement with the acquisition conditions used for the experiments shown in this work (50 nJ per pulse) in addition to two higher pump powers (100 and 150 nJ per pulse) and one lower pump power (10 nJ per pulse). All data was acquired with the same probe power, $\sim$2 nJ per pulse. Right: Linear relationship of the maximum of the transient absorption signal scaled to the minimum pump power used.

4 Data analysis methods

For the transient absorption measurements, data was gathered, as described above, as a series of phase independent lock-in amplifier amplitudes. One such measurement was performed for each pump delay value. The delay values were spaced in three segments. The first segment has linear spacing from -300 or -100 fs (depending on the measurement) to +300 fs relative to t_o. The second segment goes from 300 fs to 1 ps with logarithmic spacing and the third segment goes from 1 ps to 4 ps with logarithmic spacing. In addition to acquiring data at each delay value, after each set of delay values, the lock-in amplifiers are set to acquire at the second harmonic of the reference frequency. This measurement is also stored via the LabView program and GPIB communication and is a measurement of the total power of the probe beam to be used in calculating the transient absorbance.

The data is analyzed by first computing the change in absorbance at each delay value. This is accomplished by directly computing the following:

$$\begin{aligned}\Delta\mathrm{Abs}(t_i) &= -\log_{10}\left(\frac{I(t_i)}{I_o}\right)\\ &= -\log_{10}\left(\frac{I_o+\Delta I(t_i)}{I_o}\right)\\ &= -\log_{10}\left(1+\frac{\Delta I(t_i)}{I_o}\right)\end{aligned}$$

Where t_i is the i^{th} delay time, $\Delta\mathrm{Abs}(t_i)$ is the transient absorption signal at the delay time

t_i, I_o is the total intensity of the probe, and $\Delta I(t_i)$ is the measured change in intensity of the probe signal by the lock-in amplifier. These absorbance values, as a function of delay, are computed for the V-V, V-H, and MA data sets for each pump-probe condition and for each sample. Each set of three transient absorption decay curves is then fit with three exponential decay curves that share as global parameters the width of the convolved Gaussian (the IRF), and the time constants of decay. The relative weighting parameters for each of the three exponentials is allowed to vary for each polarization condition. The data is shown in SI figure S7 and a summary of the fitting results is shown in table S2.

5 Calculation of relative transfer rates

To estimate the relative transfer rates, we use the diagonal form of the generalized Förster theory, which accounts for the coupling between chromophores within each ring and is known to provide adequate results for LH2[1,2]. The Multi-Chromophoric Förster theory (MC-FRET) gives the resonant transfer rate between an aggregate of n_D donor molecules at equilibrium and an n_A acceptor molecules as

$$k_{DA} = \sum_{d,d'}^{n_D} \sum_{a,a'}^{n_A} V_{da} V_{d'a'} \int_{-\infty}^{\infty} d\omega \, E^D_{d'd}(\omega) I^A_{aa'}(\omega), \tag{1}$$

where the matrices $E^D(\omega)$ and $I^A(\omega)$ respectively account for the near-field emission and absorption spectra. The coupling between two chromophores separated by a distance $\vec{R}_{da}$ depends on the orientation factor $\kappa_{da} = \vec{\mu}_d \cdot \vec{\mu}_a - 3(\vec{\mu}_d \cdot \vec{R}_{da})(\vec{\mu}_a \cdot \vec{R}_{da})$, with $\vec{\mu}$ the transition dipole moments, and reads $V_{da} = K \mu_d \mu_a \kappa_{da} / R^3_{da}$, where K is a constant.

Following a series of approximations, we obtain an estimate of the pair-wise transfer rate relative to that in a reference geometry. We first make use of the weak coupling between the B800 chromophores. In first order of the coupling, the emission tensor can be replaced by the monomer spectrum $E^D_0(\omega)$, as explicit e.g. using the approximation derived in Ref.[3]. The rate of interest thus becomes

$$k_{DA} = \sum_{d}^{n_d} \sum_{\alpha}^{n_a} k_{d\alpha} = \sum_{d,\alpha} V^2_{d\alpha} \int_{-\infty}^{\infty} d\omega E^D_0(\omega) I^A_\alpha(\omega), \tag{2}$$

now written in a diagonal form using the acceptor eigenbasis, with $V_{d\alpha} = \sum_a V_{da} \langle a|\alpha\rangle$. Con-

sidering that the spectra from the different solubilization environments are only slightly shifted on the red part (Fig. 1A), we approximate the spectral overlap as constant for the considered geometries. The pair-wise transfer rate for a B800 modified geometry $k_{d\alpha}(\theta)$ relative to that of a reference geometry thus simplifies to

$$\tilde{k}_{d\alpha}(\theta) = \frac{k_{d\alpha}(\theta)}{k_{d\alpha}(0)} = \frac{V_{d\alpha}^2(\theta)}{V_{d\alpha}^2(0)}. \tag{3}$$

Using the geometry from PDB 1NKZ[4] as reference ($\theta = 0$), we obtain the direction of the transition dipole moments from the N_B to N_D atoms of each BChl. The tilt angle θ is simulated shifting the vertical position of the N_B atoms on the BChls of the B800 ring, and does not affect the B850 eigenbasis. We verify that in the B800 ring, the rate between nearest neighbors is constant across the ring due to symmetry. For a given BChl on the B800 ring, the inter-ring transfer significantly depends on which B850 BChl serves as the acceptor. Figure 4 shows the B800-B850 relative rate obtained from averaging pair-wise rates, calculated between a fixed B800 BChl and each eigenstate formed by its six nearest B850 BChls. Note that the enhancement of the B800-B850 rate mainly comes from the contribution of transfer to two BChls in the six nearest neighbours, for which the tilt drastically influences the transfer rates. Also, the B800-B850 rate is very sensitive on the distance R, and hence on the model chosen for the tilt. Disorder on the coupling can smooth this sharp dependence.[5]

6 POPC membrane discs

Membrane discs were produced using POPC to form the bilayer with the same method discussed in the main text of the paper. The purification and quantification of these discs is shown in the figure S4.

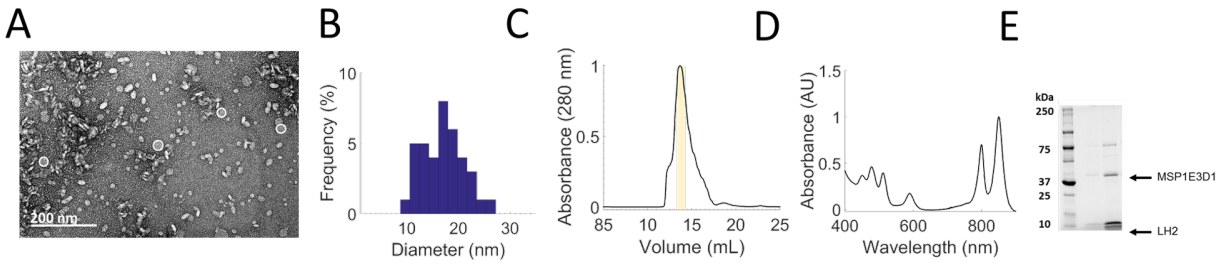

Figure 4 LH2 in discs using MSP1E3D1 and POPC. A) TEM image of FPLC purified LH2 discs. B) TEM size distribution of >100 LH2 discs. A bimodal distribution shows empty discs of 12 $\pm$ 5 nm and LH2 discs are 20 $\pm$ 5 nm. C) Size-exclusion chromatography from FPLC of LH2 discs with the LH2 disc peak highlighted in yellow. D) Absorption Spectra of LH2 in discs using POPC shows the integrity of LH2 structure. E) SDS-PAGE of LH2 peak (C) from FPLC shows both the belting protein and LH2.

7 Empty membrane discs

Empty membrane discs were produced using DMPC to form the bilayer using the same method discussed in the main text of the paper. The purification and quantification of these discs is shown in the figure S5.

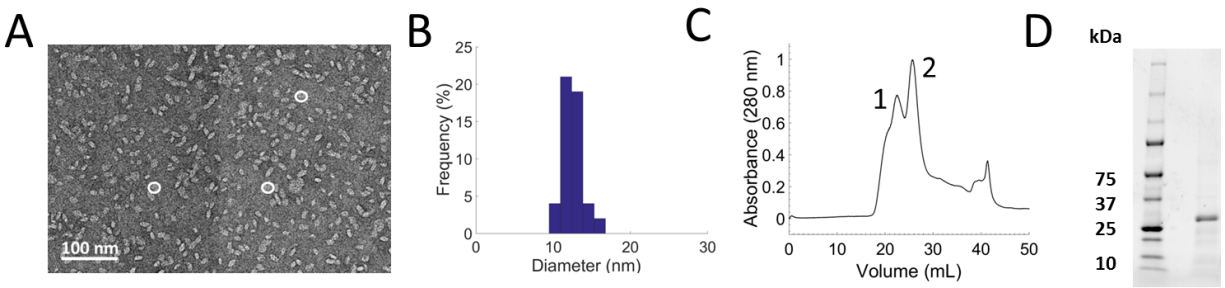

Figure 5 Empty discs using MSP1E3D1 and DMPC. A) TEM image of FPLC-purified discs (Peak 2 from C). B) TEM size distribution of >100 LH2 discs. Empty discs are 12 $\pm$ 2 nm. C) Size-exclusion chromatography from FPLC discs. Peak 2 contains discs. Fractions beyond peak 2 showed no protein on SDS-PAGE and is attributed to excess lipid. D) SDS-PAGE of Peak 2 (C) from FPLC shows only the belting protein.

8 LH2 transient absorption measurements

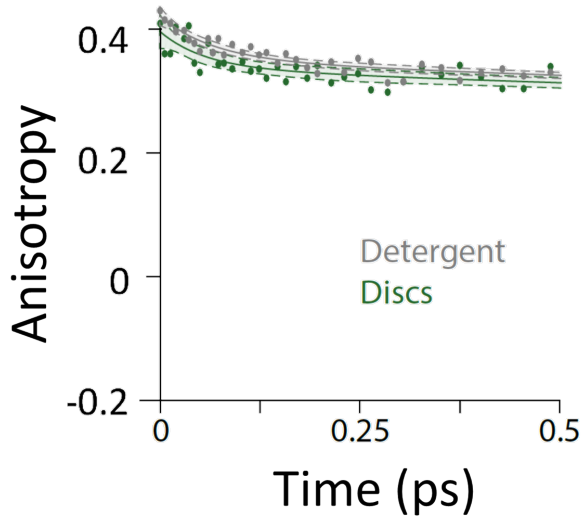

Figure 6 Anisotropy for LH2 in LDAO detergent (grey) and in DMPC discs (green) calculated from simultaneously measured parallel and perpendicular components (V-V and V-H, respectively) for 850 nm pump, 850 nm probe.

	850 Pump - 850 Probe	
	τ	Weight
Detergent	65 fs	24%
	1700 fs	53%
	>5 ns	41%
Discs	55 fs	22%
	1340 fs	31%
	> 5 ns	47%

Table 1 Anisotropy decay rates and relative weights. Each anisotropy curve was fit to a sum of three exponential decays and the time constants and relative weights of each component are shown in the table.

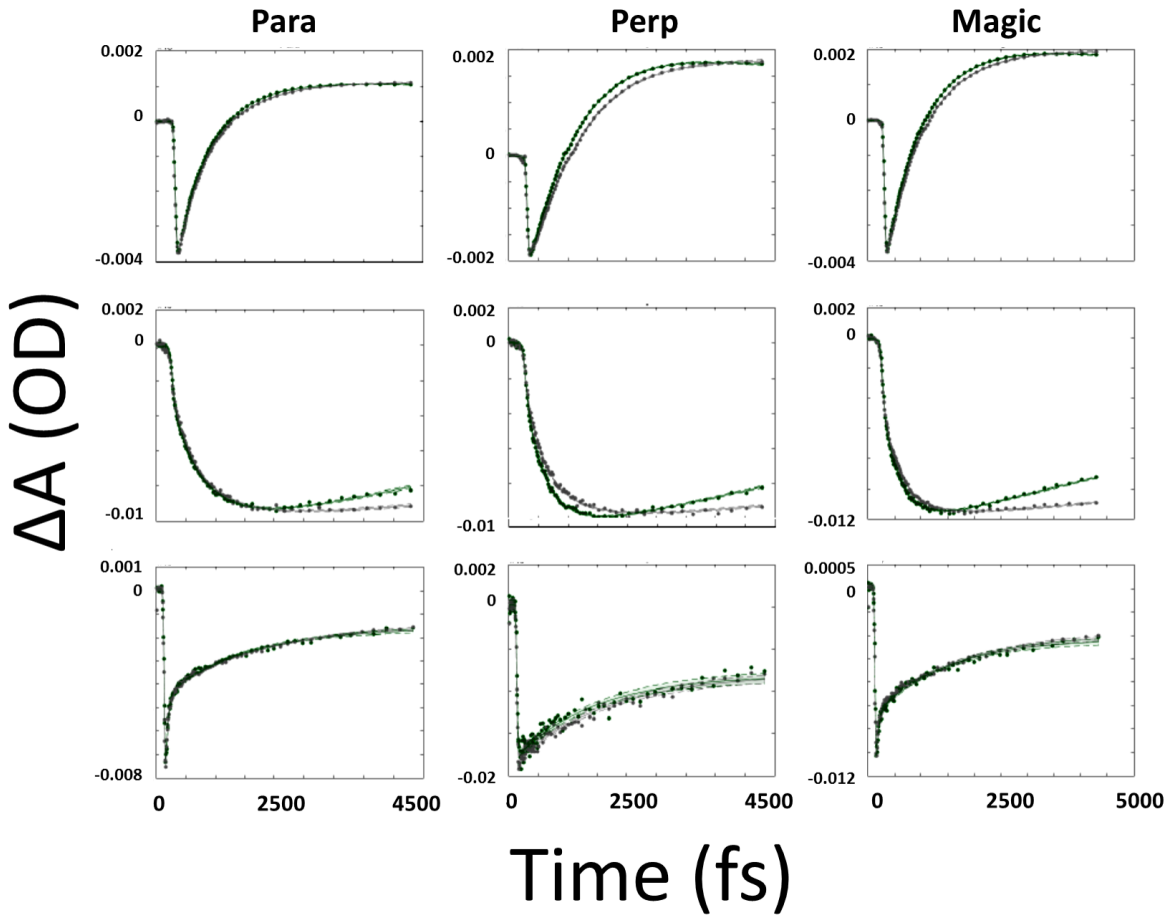

Figure 7 Pump – Probe data for LDAO solubilized LH2 (grey) and DMPC disc solubilized LH2 (green) for all illumination conditions and all polarization combinations. 800 nm – 800 nm (top row), 800 nm – 850 nm (middle row), 850 nm – 850 nm (bottom row); V-V (left column), V-H (middle column), and magic angle (right column).

	800 Pump - 800 Probe				800 Pump - 850 Probe				850 Pump - 850 Probe			
	τ	VV	VH	MA	τ	VV	VH	MA	τ	VV	VH	MA
Detergent	320 fs	-29%	5%	-14%	280 fs	10%	13%	15%	40 fs	-58%	6%	-34%
	800 fs	-49%	-64%	-58%	875 fs	36%	33%	31%	1000 fs	-20%	-29%	-26%
	13 ps	22%	31%	28%	19 ps	-54%	-54%	-54%	9.5 ps	-22%	-65%	-40%
Discs	280 fs	-18%	13%	-5%	325 fs	11%	18%	4%	33 fs	-61%	8%	-35%
	650 fs	-64%	-64%	-71%	670 fs	32%	27%	39%	900 fs	-19%	-33%	-29%
	>35 ps	18%	23%	24%	20 ps	-67%	-55%	-57%	11.5ps	-20%	-59%	-36%

Table 2 For each sample and excitation condition, the data set (V-V, V-H, and Magic Angle) was globally fit with a three exponential decay convolved with a Gaussian with duration equal to the measured IRF. The decay constants are fit globally through the data set while the relative weighting of each of the exponential decays is fit locally for each TA spectrum. This table summarizes the results for all three excitation conditions and for both the LH2 in detergent and LH2 in membrane disc samples for all three polarization conditions.

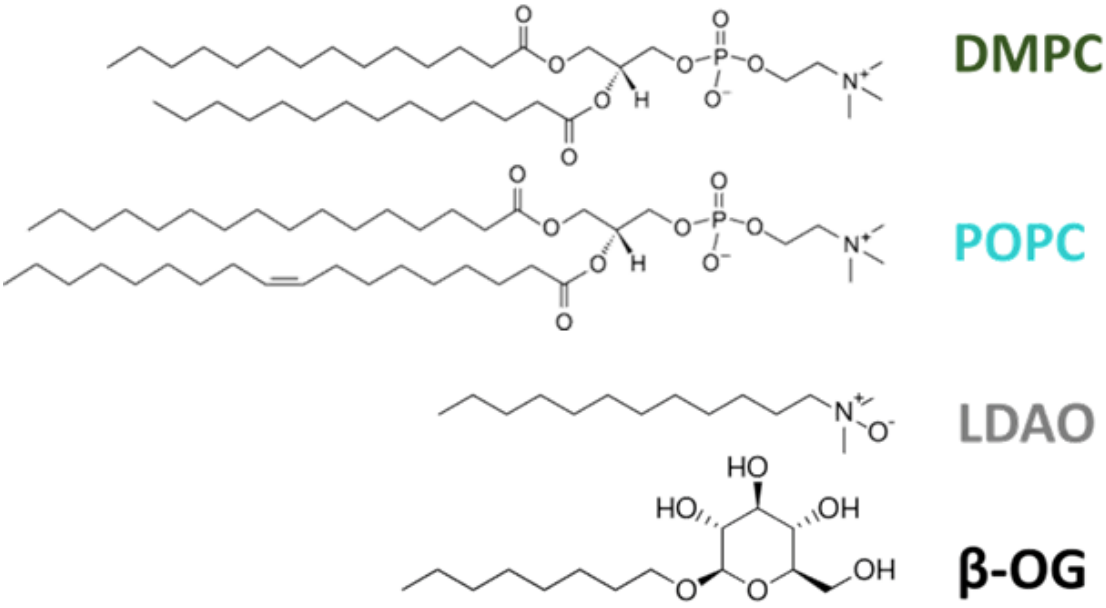

Figure 8 Lipid and detergent structures for the samples used in these experiments.

9 Time-correlated single photon counting measurements

Time-correlated single photon counting (TCSPC) experiments and curve fitting were performed as described previously[6]. For the experiments presented here, the direct output of the Ti:sapphire oscillator (Vitara-S, Coherent, Inc.) was used as the excitation source ($\lambda = 800\ nm$, $80\ MHz$). The excitation wavelength was selected with a 800 nm center-wavelength bandpass (FF01-7851/62-25, Semrock Inc.). The emission wavelength was selected with a 875 center-wavelength bandpass filter (FF01-834/LR 25-L2, Semrock Inc.). Excitation density for these experiments was 6.22 mW/cm^2

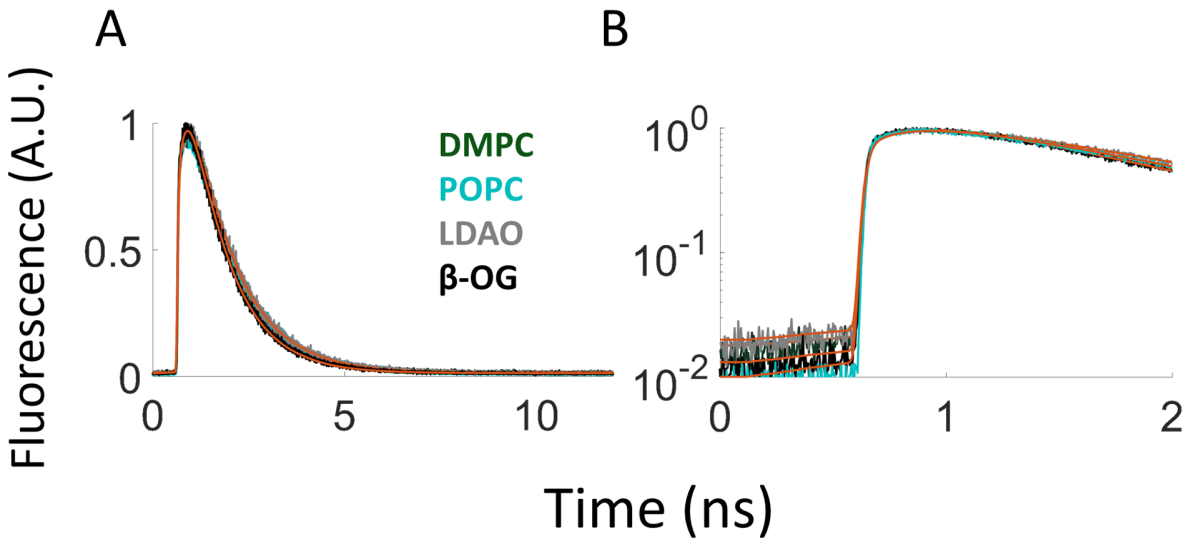

Figure 9 Fluorescence lifetime data for all four samples in A) full linear scale and B) logarithmic scale to 2 ns. Data is shown in color and fits are shown as red lines. All samples were fit to a mono-exponential decay.

	TCSPC	
	A1	τ1
β-OG	1	1.018 ns
LDAO	1	1.113 ns
DMPC	1	1.119 ns
POPC	1	0.974 ns

Table 3 Parameters extracted from fits of the TCSPC data. Each fluorescence decay curve was fit mono-exponentially. The amplitudes and time constants are shown.

References

[1] K. Mukai, S. Abe and H. Sumi, *The Journal of Physical Chemistry B*, 1999, **103**, 6096–6102.

[2] S. Jang, M. D. Newton and R. J. Silbey, *Physical review letters*, 2004, **92**, 218301.

[3] A. Chenu and J. Cao, *Physical review letters*, 2017, **118**, 013001.

[4] M. Z. Papiz, S. M. Prince, T. Howard, R. J. Cogdell and N. W. Isaacs, *Journal of molecular biology*, 2003, **326**, 1523–1538.

[5] L. Cleary and J. Cao, *New Journal of Physics*, 2013, **15**, 125030.

[6] J. L. Banal, T. Kondo, R. Veneziano, M. Bathe and G. S. Schlau-Cohen, *The journal of physical chemistry letters*, 2017, **8**, 5827–5833.